Original Article

Aberrant Global and Regional Topological Organization of the Fractional Anisotropy-weighted Brain Structural Networks in Major Depressive Disorder

Jian-Huai Chen[1], Zhi-Jian Yao[1], Jiao-Long Qin[2], Rui Yan[1], Ling-Ling Hua[1], Qing Lu[2,3]

[1]Department of Psychiatry, Affiliated Nanjing Brain Hospital, Nanjing Medical University, Nanjing, Jiangsu 210029, China
[2]Research Center of Learning Science, Southeast University, Nanjing, Jiangsu 210096, China
[3]Research Institute of Suzhou, Southeast University, Suzhou, Jiangsu 215123, China

Abstract

Background: Most previous neuroimaging studies have focused on the structural and functional abnormalities of local brain regions in major depressive disorder (MDD). Moreover, the exactly topological organization of networks underlying MDD remains unclear. This study examined the aberrant global and regional topological patterns of the brain white matter networks in MDD patients.
Methods: The diffusion tensor imaging data were obtained from 27 patients with MDD and 40 healthy controls. The brain fractional anisotropy-weighted structural networks were constructed, and the global network and regional nodal metrics of the networks were explored by the complex network theory.
Results: Compared with the healthy controls, the brain structural network of MDD patients showed an intact small-world topology, but significantly abnormal global network topological organization and regional nodal characteristic of the network in MDD were found. Our findings also indicated that the brain structural networks in MDD patients become a less strongly integrated network with a reduced central role of some key brain regions.
Conclusions: All these resulted in a less optimal topological organization of networks underlying MDD patients, including an impaired capability of local information processing, reduced centrality of some brain regions and limited capacity to integrate information across different regions. Thus, these global network and regional node-level aberrations might contribute to understanding the pathogenesis of MDD from the view of the brain network.

Key words: Diffusion Tensor Imaging; Graph Theory Analysis; Major Depressive Disorder; Topological Organization

Introduction

Major depressive disorder (MDD) is one of the most common and costly psychiatric disorders, which is characterized by pervasive feelings of sadness, anxiety, low self-esteem, and social behavior abnormalities.[1,2] With this mental disorder, most of the MDD patients suffer more than one recurrence of depressive episodes with a greater chance of suicide, which results in a yearly increasing morbidity and a high risk of mortality of MDD.[3]

Recently, neuroimaging studies have documented that MDD is associated with widespread structural and functional brain change.[4,5] For example, functional and structural neuroimaging studies have shown abnormal neural activities and microstructural abnormalities in many local brain regions, such as the prefrontal cortex, orbitofrontal cortex, anterior cingulated cortex, amygdala, the hippocampus, parahippocampal gyrus, insula, basal ganglia, and the temporal, occipital regions.[6-9] However, most of these studies focus on locally specific regions in the brain of MDD patients.[10,11] And recent advances in the modern neuroimaging technique of diffusion tensor

Access this article online

Quick Response Code:

Website: www.cmj.org

DOI: 10.4103/0366-6999.178002

Address for correspondence: Dr. Zhi-Jian Yao, Department of Psychiatry, Affiliated Nanjing Brain Hospital, Nanjing Medical University, Nanjing, Jiangsu 210029, China
E-Mail: zjyao@njmu.edu.cn

This is an open access article distributed under the terms of the Creative Commons Attribution-NonCommercial-ShareAlike 3.0 License, which allows others to remix, tweak, and build upon the work non-commercially, as long as the author is credited and the new creations are licensed under the identical terms.

For reprints contact: reprints@medknow.com

© 2016 Chinese Medical Journal ¦ Produced by Wolters Kluwer - Medknow

Received: 01-11-2015 **Edited by:** Xiu-Yuan Hao and Li-Min Chen
How to cite this article: Chen JH, Yao ZJ, Qin JL, Yan R, Hua LL, Lu Q. Aberrant Global and Regional Topological Organization of the Fractional Anisotropy-weighted Brain Structural Networks in Major Depressive Disorder. Chin Med J 2016;129:679-89.

imaging (DTI) have allowed for noninvasive investigation of the orientation and integrity of white matter (WM) fiber bundles.[12] Based on these advances, there is an increasing of evidence suggesting that the mechanism underlying the locally functional and structural abnormalities in the brain of MDD patients may be associated with the reduction of oligodendrocytes and the decreased myelin-related gene expression, which result in the widespread disruptions of WM integrity.[13] Considering these distributed functional and structural abnormalities among a variety of brain areas and the impaired integrity of the WM tracts between them, MDD is recognized as a disconnection psychiatric disorder.[14] So, characterization of the global architecture consisted of the regional brain areas and the functional or structural connectivity between them is crucial in the brain of MDD patients. It could increase our understanding of the pathophysiology underlying MDD from the view of the large-scale organization of structural connectivity that underlie functional states.

Recent research has suggested that graph-based network analysis is a powerful method that allow us to quantifying the organization of brain connectivity and characterize topological properties of brain networks by mapping the brain as a functional or structural networks consisting of nodes (i.e., brain regions or voxels) and edges (i.e., functional or structural connectivity between regions).[15-17] MDD is conceptualized as a network-level disease with the disruption of the topological organization of the brain functional and gray matter volume based networks in recent studies.[18-21] These studies on the functional and structural brain networks based on gray matter volume or cortical thickness had found that the brain structural networks in both healthy controls (HCs) and MDD patients followed an efficient small-world organization. However, some abnormalities of global topological properties in the brain networks of MDD patients were also reported, such as the clustering coefficient, the characteristic path length, the local and global efficiency. Until date, little is known about the differences of the organizational patterns of the brain WM networks between MDD patients and HCs. No study has directly examined the topological organization of WM networks of MDD patients.

In this study, we aimed to investigate topological properties of the brain WM structural networks in MDD patients, combining DTI with graph theory analysis from an integrative systems perspective. Here, we tested that whether the brain WM network of MDD patients has a small-world architecture as the same with that in HCs. And then, we focus on other related metrics (i.e., betweenness, hubs, efficiency) that characterizes the differences of the pattern and efficiency of the information communicating and metrics that quantify the segregated and integrative connectivity patterns (the local density of connections within regions, clustering; the integrative connectivity patterns between regions, path length) between MDD patients and HCs.

Methods

Subjects

Twenty-seven patients with unipolar MDD (right-handed; 10 male and 17 female; age: 32.96 ± 8.84 years) were recruited for this study from part of a large cohort of depression patients in the Chinese population of Han nationality in the inpatient Department of Affiliated Brain Hospital of Nanjing Medical University, China. The psychiatric diagnoses of all the patients were made according to the Structured Clinical Interview for DSM Disorders. All patients were currently experiencing an episode of depression with the 17-item Hamilton rating scale for depression total score ≥17 that was rated by an experienced psychiatrists on the day of image acquisition. All patients with other Axis I psychiatric disorders and symptoms or a history of electroconvulsive therapy were excluded.

Forty age-, and sex-matched healthy subjects (right-handed; 21 male and 19 female; age: 31.43 ± 7.80 years) served as controls were recruited by media advertisements from the similar geographic and demographic regions. HC subjects with a psychiatric illness history or any family history of major psychiatric diseases in their first-degree relatives were excluded.

All subjects met the exclusion criteria: (1) a history of alcohol or drug dependence; (2) a history of brain disorder, neurological disorders, or cardiovascular diseases; (3) any serious physical illness as assessed by personal history and laboratory analysis; (4) currently pregnancy or breastfeeding; and (5) the inability to undergo an magnetic resonance imaging (MRI). The protocol was approved by the Ethics Committee of the Affiliated Nanjing Brain Hospital of Nanjing Medical University and written informed consent was obtained from all subjects. The demographic and clinical characteristics of these subjects are presented in Table 1.

Image acquisition

MRI was acquired using a 3.0-Tesla Siemens Verio MRI Scanner (Siemens AG, Erlangen, Germany) in the Affiliated

Table 1: Demographic and clinical characteristics of MDD patients and healthy controls

Variables	Group		t/χ^2	*P*
	HC	MDD		
Sample size, *n*	40	27	–	–
Age, years (mean ± SD)	31.43 ± 7.80	32.96 ± 8.84	−0.75	0.46*
Gender, *n* (male/female)	21/19	10/17	1.55	0.21†
Handedness, *n* (right/left)	40/0	27/0	–	–
Number of previous episodes (mean ± SD)	–	1.63 ± 1.08	–	–
Duration of illness, months (mean ± SD)	–	4.26 ± 3.51	–	–
Score of 17-item HAMD (mean ± SD)	–	26.22 ± 4.54	–	–

*The *P* value was obtained by two-sample two-tailed *t*-test; †The *P* value was obtained by Pearson Chi-square test. The *P* value more than 0.05 indicated no statistically significant difference between the two groups. HC: Healthy controls; MDD: Major depressive disorder patients; HAMD: Hamilton Depression Rating Scale; SD: Standard deviation.

Nanjing Brain Hospital of Nanjing Medical University. During the scan, all subjects were instructed to relax with their eyes closed and not think of anything in particular but not to fall asleep. T1-weighted images: Repetition time (TR) = 1900 ms, echo time (TE) = 2.48 ms, thickness/gap = 1.0/0 mm, flip angle = 9°, inversion time = 900 ms. DTI was acquired: TR = 6600 ms, TE = 93 ms, thickness/gap = 3/3 mm, flip angle = 90°, 30 diffusion directions with $b = 1000$ s/mm^2, and an additional image without diffusion weighting (i.e., $b = 0$ s/mm^2).

Data preprocessing

All diffusion images were preprocessed with the Functional Magnetic Resonance Imaging of the Brain Software Library-FMRIB's Diffusion Toolbox (http://www.fmrib.ox.ac.uk/fsl/fdt/index.html). All images were first corrected for distortions due to eddy current and simple head motions with the FSL toolbox, then estimate the diffusion tensor and calculate the fractional anisotropy (FA). And the baseline $b = 0$ images of all participants were normalized to the T1-weighted image using a linear transformation, and then registered to the standard FA template in the Montreal Neurological Institute (MNI) 152 standard space (MNI-152 space). Using the transformation matrices created in the above two register processing steps, the resulting transformation matrix from diffusion space to MNI space was calculated and then stored for later use.

In addition, we reconstructed WM bundles in the whole brain of each subject with Diffusion Toolkit (http://www.trackvis.org) toolbox, to generate the three-dimensional curves characterizing corticocortical fiber tract connectivity and to reconstruct WM tracts of the brain network based on the diffusion map of each individual. For each individual dataset, each streamline was propagated using the fiber assignment by continuous tracking algorithm.[22]

Network construction

A network can be constructed by defining nodes and estimating edges. The definition of nodes and edges is important in the brain network construction as they are the most basic elements of a network. In this study, the procedure that we undertook to define the nodes and edges in each network is similar to that used in previous studies[23] and described as follows. All the processing pipelines were presented in Figure 1.

Network node definition

To construct the brain structural networks in this study, we firstly employed an automated structural labeling template[24] to parcellate the entire brain into 90 cortical regions (45 for each hemisphere), each cortical or subcortical region representing a node of the cortical network by the graph theoretic approach that has been described previously.[25] Note that, in our case, the cerebellums were removed and the names of the regions of interests and their corresponding abbreviations are listed in Table 2.

Table 2: Cortical and sub-cortical regions as anatomically defined in the AAL template and their corresponding abbreviations

Region name	Abbreviation
Precentral gyrus	PreCG
Postcentral gyrus	PosCG
Rolandic operculum	ROL
Superior frontal gyrus, dorsolateral	SFGdor
Superior frontal gyrus, orbital	SFGorb
Superior frontal gyrus, medial	SFGmed
Superior frontal gyrus, medial orbital	SFGmedorb
Middle frontal gyrus	MFG
Middle frontal gyrus, orbital	MFGorb
Inferior frontal gyrus, opercular	IFGoper
Inferior frontal gyrus, triangular	IFGtri
Inferior frontal gyrus, orbital	IFGorb
Supplementary motor area	SMA
Olfactory cortex	OLF
Gyrus rectus	GRE
Paracentral lobule	PCL
Heschl gyrus	HES
Superior temporal gyrus	STG
Middle temporal gyrus	MTG
Inferior temporal gyrus	ITG
Superior parietal gyrus	SPG
Inferior parietal, but supramarginal and angular gyri	IPL
Supramarginal gyrus	SMG
Angular gyrus	ANG
Precuneus	PCUN
Calcarine fissure and surrounding cortex	CAL
Cuneus	CUN
Lingual gyrus	LING
Superior occipital gyrus	SOG
Middle occipital gyrus	MOG
Inferior occipital gyrus	IOG
Fusiform gyrus	FFG
Anterior cingulate and paracingulate gyri	ACG
Median cingulate and paracingulate gyri	DCG
Posterior cingulate gyrus	PCG
Hippocampus	HIP
Parahippocampal gyrus	PHG
Temporal pole: superior temporal gyrus	TPOstg
Temporal pole: middle temporal gyrus	TPO
Amygdala	AMY
Caudate nucleus	CAU
Lenticular nucleus, putamen	PUT
Lenticular nucleus, pallidum	PAL
Thalamus	THA
Insula	INS

AAL: Automated anatomical labeling.

Network edge definition

We determined the edges of the brain structural network by using the corticocortical fiber tract connectivity dataset of each individual. The fiber bundle was modeled as the edge between nodes i and j (i.e., brain region i and region j) when it was considered to link these two brain regions with both of the fiber bundle's endpoints adjacent to the two brain regions. This procedure was repeated for all brain regions i and j in the whole cerebral cortex. And then the resulting matrix (network, or graph) would be constructed, which represents the undirected brain structural network, comprising a total of 90 nodes that are structurally

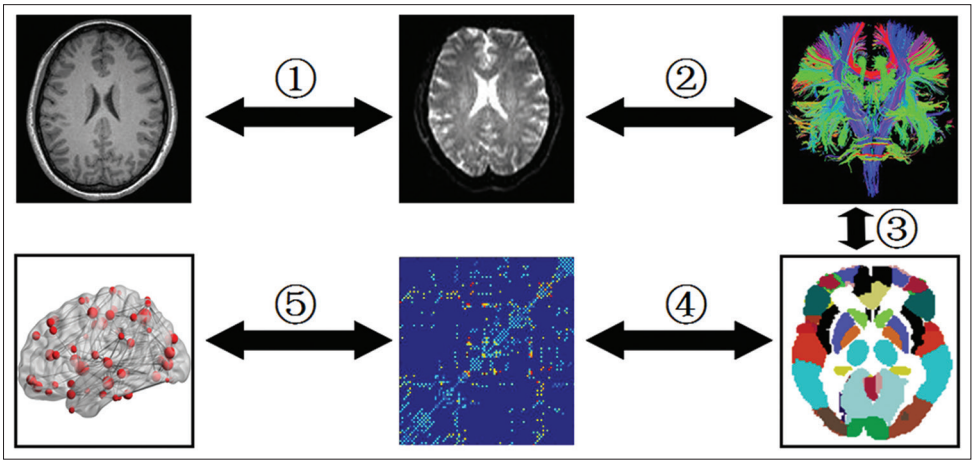

Figure 1: A flowchart of brain white matter structural network construction. (1) The T1-weighted images were registered to the corresponding nondiffusion-weighted (b = 0) images. (2) The white matter fiber bundles in the whole brain were define by using diffusion tensor imaging deterministic tractography. (3) The entire brain was parcellated into 90 cortical regions and each region represented a node of the cortical network by using the automated structural labeling template. (4) The resulting weighted matrix would be constructed by calculating the mean fractional anisotropy values of the connected streamlines between regions as the weights of the network edges. (5) The weighted brain white matter structural network was constructed for each participant with the regions of interests becoming nodes and the fibers transformed into edges in the network.

connected and the connections between these nodes. The weighted network analyses were performed after the matrix constructed. We calculated the mean FA values of the connected streamlines between two regions by the average of FA values of all voxels on each fiber track as the weights of the network edges. As a result, we obtained a weighted structural network for each participant.

Network analysis

We calculated both global and regional metrics of the brain networks in Matlab using the Brain Connectivity Toolbox.[17]

Global network metrics

The global topological properties of network were characterized by the global network metrics, including five key small-world parameters[26] (the average clustering coefficient C, the average characteristic path length L, the average normalized clustering coefficient γ, the average normalized shortest path length λ, and the small-worldness σ), four network efficiency parameters[27] (the average local efficiency E_{loc}(real), the average global efficiency E_{glob}(real), the average normalized local efficiency E_{loc}(normal), the average normalized global efficiency E_{glob}(normal), and the average connection strength.[28]

Weighted clustering coefficient

Briefly, the clustering coefficient is a measure of network segregation. C (i) quantifies the likelihood of whether the neighborhoods were connected with each other or not and C indicates the extent of the local cliquishness and local efficiency of information transfer. In a weighted graph G with N nodes, the C (i) for node i is defined as the ratio of the number of existing connections between its nearest neighbors to the number of all possible: $C(i)^{\text{weighted}} = \frac{\sum_{j,k \in G(i)} (w_{ij} w_{ik} w_{jk})^{1/3}}{K(i)(K(i)-1)}$, where w_{ij} is the weight between node i and j in the network, G (i) denotes the subgraph composed of the nearest neighbors of node i and K (i) is the number of edges in the subgraph G (i). Obviously, the clustering coefficient C of the graph G is the average of the clustering coefficient over all nodes in a network. Formally: $C(G)^{\text{weighted}} = \frac{1}{N}\sum_{i \in N} C(i)^{\text{weighted}}$.

Weighted characteristic path length

The path length between nodes i and j is defined as the sum of the edge lengths along this path. The characteristic path length between node i and j is defined the smallest number of edges connecting them. For weighted networks, the length of each edge was assigned by computing the reciprocal of the edge weight $1/w_{ij}$. The characteristic path length L quantifies the ability of parallel information propagation or global efficiency of information transfer of a network, which is the most commonly used measure of network integration. In a weighted graph G with N nodes, the characteristic path length of a node is the average value of shortest path length from node i to all other nodes in the network: $L(i)^{\text{weighted}} = \frac{\sum_{i \neq j \in N} d^{\text{weighted}}(i,j)}{N-1}$, where $d(i,j)^{\text{weighted}} = \sum_{w_{km} \in gi \leftrightarrow j^{\text{weighted}}} 1/w_{km}$, is the shortest path length between node i and j in G; $gi \leftrightarrow j$ is the shortest weighted distance between node i and j in the graph G that cross on the way nodes u and v and w_{uv} is defined as the weight of the connection between node u and node v. The characteristic path length L of the network is the average of characteristic path length between all node pairs in the network: $L(G)^{\text{weighted}} = \frac{1}{N}\sum_{i \in N} L(i)^{\text{weighted}}$.

Weighted local efficiency

In a weighted graph G with N nodes, the local efficiency of each node could be calculated as the global efficiency of the neighborhood subgraph $G(i)$ of the node: $E_{loc}(i)^{weighted} = \frac{\sum_{j\neq k\in G(i)} \left\{a_{ij}a_{ik}[d_i(jk)^{weighted}]^{-1}\right\}^{1/3}}{K(i)K(i)-1}$, where $G(i)$ denotes the subgraph composed of the nearest neighbors of node i, $d_i(jk)^{weighted}$ is the shortest path length between node j and k in $G(i)$. And the network local efficiency E_{loc} of G is defined as the average of those of all nodes within the network, which represents how much the network is fault tolerant and shows how efficient the information is communicated within the neighbors of a given node when this node is removed. Formally: $E_{loc}(G)^{weighted} = \frac{1}{N}\sum_{i\in G(i)} E_{loc}(i)^{weighted}$.

Weighted global efficiency

The global efficiency of the graph G measures the efficiency of the parallel information transfer in the network. And the global efficiency of node i is defined as follows: $E_{glob}(i)^{weighted} = \frac{\sum_{j\neq k\in G}[d(ij)^{weighted}]^{-1}}{N-1}$, where $d(ij)^{weighted}$ is the shortest path length between node i and j in G. Obviously, the average global efficiency of the network is defined as the reciprocal of the average of the reciprocals of shortest path length between pairs of nodes within the network. Formally: $E_{glob}(G)^{weighted} = \frac{1}{N}\sum_{i\in G} E_{glob}(i)^{weighted}$.

Weighted strength

For a weighted graph G with N nodes, we calculated the $S(i)$ of node i by the sum of the edge weights w_{ij} linking to node i. Formally: $S(i) = \sum_{j\in G} w_{ij}$, where w_{ij} was the weight between node i and node j in the graph G. Obviously, the S of the graph G is the average of the strength across all of the nodes in the network. Formally: $S(G) = \frac{1}{N}\sum_{i\in G} S(i)$.

Small-world properties

To explore the small-world topological properties of the networks, we compared the values of C(rand) and L(rand) of the network with those of 100 random networks. The random networks were constructed by using the random rewiring procedure, which preserve the same number of nodes, edges, and degree distribution as the real networks whereas the corresponding weights are redistributed.[29] And then the normalized clustering coefficient $\gamma = C(real)/C(rand)$ and the normalized characteristic path length $\lambda = L(real)/L(rand)$ were computed (C(real) and L(real) are the clustering coefficient and the characteristic path length of real networks, and C(rand) and L(rand) represent the means of corresponding indices derived from 100 matched random networks). Compared with random networks, small-world networks have similar characteristic path length but higher clustering coefficient, that means a small-world network not only has a higher level of local interconnectivity or local efficiency of information transfer but also has an approximately equivalent shortest path length or higher global efficiency of information transfer compared with random networks ($\gamma = C(real)/C(rand) >> 1 >> 1$, $\lambda = L(real)/L(rand) \approx 1$) (Watts and Strogatz, 1998). These two metrics can also be summarized into a simple quantitative measurement, small-worldness $\sigma = \gamma/\lambda \geq 1$.[30]

Small-world efficiency

To explore the small-world efficiency, we also compared the values (E_{glob} and E_{loc}) of the networks with those of 100 random networks, which also preserve the same number of nodes, edges, and degree distribution as the real networks whereas the corresponding weights are redistributed.[29] A real network would be considered to have small-world efficiency if $E_{loc}(normal) = E_{loc}(real)/E_{loc}(rand) >> 1$ and $E_{glob}(normal) = E_{glob}(real)/E_{glob}(rand) \approx 1$ (E_{loc}(real); E_{glob}(real) and E_{loc}(rand); E_{glob}(rand) were the average global efficiency E_{glob} and the average local efficiency E_{loc} of the brain structural networks and their 100 matched random networks respectively.[26] Namely, a small-world network not only has a higher level of local efficiency but also has an approximate level of global efficiency compared with the random networks (i.e., very efficient both in global and local information transfer).[31]

Regional network metrics

The topological properties of nodes were characterized by the regional node measures, including the clustering coefficient $C(i)$, the characteristic path length $L(i)$, global efficiency $E_{glob}(i)$, local efficiency $E_{loc}(i)$ and two nodal centrality parameters: the strength $S(i)$ and normalized betweenness $b(i)$.

Weighted betweenness centrality

In a weighted graph G with N nodes, the betweenness centrality $B(i)$ of a node i is calculated as the fraction of shortest paths between pairs of other nodes that pass through the node i, which representing that the central node i plays a pivotal role in control over the information transfer within the graph. $B(i)$ of a node i is centrality measures that capture the influence of the node i over information flow between other nodes in the network. In this study, we calculated the normalized betweenness centrality $b(i)$ of a node i as $b(i) = B(i)/<B(i)>$ (where $<B(i)>$ is the average nodal betweenness of the network).[17] Formally: $b(i) = \sum_{i\neq j\neq k\in G} \frac{\sigma_{jk}(i)}{\sigma_{jk}}$, where $\sigma_{jk}(i)$ is the number of shortest

path between node j and node k passing through node i, σ_{jk} is the number of shortest path between node j and node k.

Hubs of the weighted network

Hubs of the weighted network indicate the contribution of nodes to facilitate global integrative processes within the cerebral cortex.[32] The nodes with the largest normalized betweenness b (i) or the strength S (i) were considered pivotal nodes (i.e., hubs) in the network. Specifically, nodes were identified as the hubs in the cortical network if their normalized betweenness b (i) or the strength S (i) were at least one standard deviation (SD) greater than the average normalized betweenness b (i) or strength S (i) of the network (i.e., b (i) > mean + SD or S (i) > mean + SD)).

Statistical analysis

Differences in global network metrics

For global network metrics (the average clustering coefficient C, the average characteristic path length L, the average local E_{loc}(real) and global efficiency E_{glob}(real), the average strength S), a two-sample two-tailed t-test was separately performed to determine the significant between-group differences on each network metric. A significant threshold of P = 0.05 was used for testing the overall level network characteristics.

Differences in regional nodal metrics

For regional nodal metrics (the clustering coefficient C (i), the characteristic path length L (i), the local E_{loc}(i) and global efficiency E_{glob}(i), the strength S (i) and the betweenness b (i)), a two-sample two-tailed t-test was also separately performed to determine the significant between-group differences on each nodal metric. To address the problem of multiple comparisons in the regional nodal metrics and maintain an experiment-wise error rate of 0.05, a false discovery rate (FDR) correction was employed to address the problem with the threshold of P = 0.05, where the number of comparisons was 90.

Results

Global network analyses

Small-worldness

Both HCs and MDD patients showed a small-world organization of the brain structural networks expressed by $\gamma = C_{real}/C_{rand} >> 1$ (HC: 4.65 ± 0.44; MDD: 4.88 ± 0.56) and $\lambda = L_{real}/L_{rand} \approx 1$ (HC: 0.84 ± 0.03; MDD: 0.83 ± 0.02). This pattern resulted in $\sigma \geq 1$ in both groups. The results suggested that there were small-world characteristics of the brain structural networks in both groups [Figure 2a and Table 3].

Small-world efficiency

Using small-world efficiency analyses, we found that the brain structural networks of both HCs and MDD patients exhibited a similar global efficiency and a much higher local efficiency compared with the matched random networks (HC: E_{loc}(normal) = 4.74 ± 0.87, E_{glob}(normal) = 0.89 ± 0.02; MDD: E_{loc}(normal) = 5.24 ± 0.95, E_{glob}(normal) = 0.88 ± 0.02). The results also suggested that there were small-world characteristics of the brain structural networks in both groups from the view of the efficiency of the brain structural network [Figure 2b and Table 3].

Table 3: The results of the small-worldness and small-efficiency in healthy controls and MDD patients

Variable	Group	
	HC	MDD
The small-worldness		
The normalized clustering coefficient (γ)	4.65 ± 0.44	4.88 ± 0.56
The normalized characteristic path length (λ)	0.84 ± 0.03	0.83 ± 0.02
The small-worldness (σ)	5.58 ± 0.63	5.93 ± 0.75
The small-efficiency		
$E_{loc}(normal) = E_{loc}(real)/E_{loc}(rand)$	4.74 ± 0.87	5.24 ± 0.95
$E_{glob}(normal) = E_{glob}(real)/E_{glob}(rand)$	0.89 ± 0.02	0.88 ± 0.02
$E_{loc}(normal)/E_{glob}(normal)$	5.32 ± 1.02	5.95 ± 1.15

E_{loc}(real), E_{glob}(real) and E_{loc}(rand), E_{glob}(rand) were the average local and global efficiency of the brain anatomical networks and the 100 matched random networks respectively. E_{loc}(normal): The normalized average local efficiency; E_{glob}(normal): The normalized average global efficiency. HC: Healthy controls; MDD: Major depressive disorder patients.

Alterations in global network metrics

Compared with HCs, MDD patients decreased in the clustering coefficient C (P = 0.018), the average local efficiency E_{loc}(real) (P = 0.025), the average global efficiency E_{glob}(real) (P = 0.0035) and the average strength S (P = 0.015) of the brain structural network [Table 4].

Regional nodal analyses

Identification of Hubs

To identify the hub regions in the network, we examined the normalized betweenness b (i) and the strength S (i) centrality of each cortical region in cortical networks of both groups. A given region in a network was defined as a hub if its normalized betweenness b (i) or S (i) was, at least, one SD greater than the average betweenness or strength of the network. In the HC group, 13 regions were identified as the hubs by the normalized betweenness b (i) and 18 regions by the strength S (i). In the MDD group, 12 regions were identified as the hubs by the normalized betweenness b (i) and 15 regions by the strength. And the hubs identified by both b (i) and S (i) in HCs were the left and right precentral gyrus, left and right calcarine fissure and surrounding cortex, left and right insula and left median cingulate and paracingulate gyri. The hubs identified by both b (i) and S (i) in MDD patients were the left and right precentral gyrus, left calcarine fissure and surrounding cortex, left and right insula and left median cingulate, paracingulate gyri [Figure 3 and Table 5].

Alterations in regional nodal characteristics

Compared with HCs, MDD patients showed decreased nodal global efficiency in brain regions, including the right rolandic operculum (P = 0.00013*), the right supramarginal gyrus

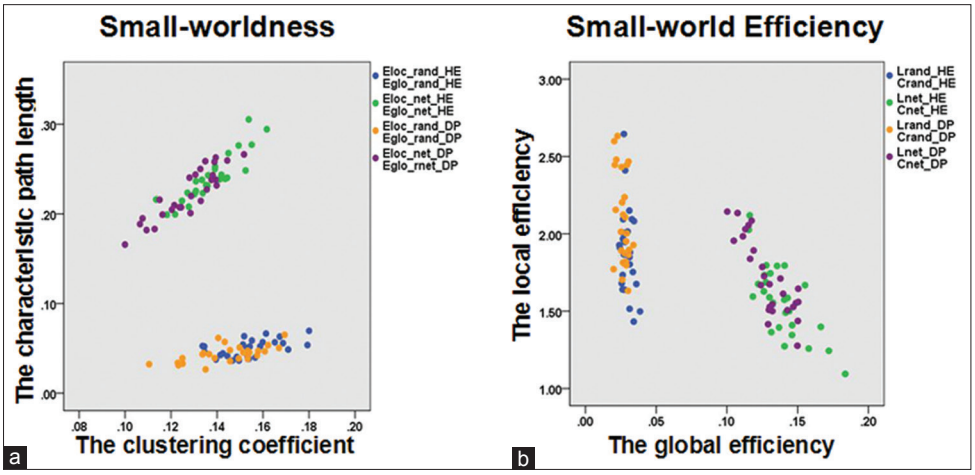

Figure 2: The small-worldness and small-world efficiency of the brain structural networks of healthy controls and major depressive disorder patients. E_{loc} and E_{glo} respectively represent the local and global efficiency; *C* and *L* respectively represent the clustering coefficient and characteristic path length; *net* and *rand* respectively represent the brain network and rand network. (a) Both of healthy controls and major depressive disorder patients have a similar characteristic path length and a much higher clustering coefficient when compared with the matched random networks. The normalized characteristic path length $\lambda \approx 1$ and the normalized clustering coefficient $\gamma >> 1$. (b) Both of healthy controls and major depressive disorder patients have a similar global efficiency and a much higher local efficiency compared with the matched random networks.

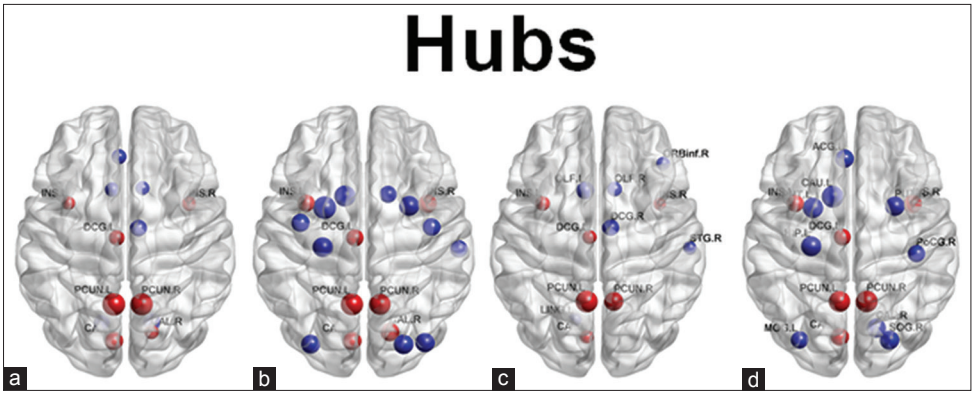

Figure 3: Hub regions in the brain structural networks of healthy controls and major depressive disorder patients. All the names of the brain regions in Figure 3 please refer to Table 2. Nodes represented brain regions, and the size of the nodes (i.e., diameter) represented the magnitude of the normalized betweenness *b* (*i*) or the strength *S* (*i*). (a) The hubs defined by the normalized betweenness *b* (*i*) in the brain structural networks of healthy controls. (b) The hubs defined by the strength *S* (*i*) in the brain structural networks of healthy controls. (c) The hubs defined by the normalized betweenness *b* (*i*) in the brain structural networks of major depressive disorder patients. (d) The hubs defined by the strength *S* (*i*) in the brain structural networks of major depressive disorder patients. Hubs in red mean those identified by both *b* (*i*) and *S* (*i*) in healthy controls or major depressive disorder patients.

Table 4: Abnormal overall level network metrics in healthy controls and MDD patients

Variable	Group		*t*	*P*
	HC	MDD		
The clustering coefficient (*C*)	0.14 ± 0.02	0.13 ± 0.02	2.42	0.018
The characteristic path length (*L*)	1.61 ± 0.24	1.71 ± 0.24	−1.68	0.099
The average local efficiency (E_{loc}(real))	0.24 ± 0.03	0.22 ± 0.03	2.29	0.025
The average global efficiency (E_{glob}(real))	0.14 ± 0.01	0.13 ± 0.01	3.03	0.004
The average strength (*S*)	2.41 ± 0.23	2.25 ± 0.27	2.49	0.015

The *P* value was obtained by two-sample two-tailed *t*-test. The *P* value was obtained by two-sample two-tailed *t*-test (significant between-group differences were shown in bold font). HC: Healthy controls; MDD: Major depressive disorder.

($P = 0.00036$*), the right angular gyrus ($P = 0.000064$*), the right Heschl's gyrus ($P = 0.00018$*) and the left middle temporal gyrus (temporal pole) ($P = 0.00026$*) (*indicated that the regions survived critical FDR threshold for multiple comparisons). However, the between-group differences in the nodal local efficiency $E_{loc}(i)$, clustering coefficient $C(i)$, characteristic path length $L(i)$, strength $S(i)$ and normalized betweenness $b(i)$ did not survived critical FDR

Table 5: Regions identified as hubs in the networks of healthy controls and MDD patients

HC						MDD					
Regions		Average *b* (*i*)	Regions		Average *S* (*i*)	Regions		Average *b* (*i*)	Regions		Average *S* (*i*)
PCUN	Left	4.24	PUT	Left	4.73	PCUN	Left	4.27	CAU	Left	4.37
PCUN	Right	4.11	PCUN	Left	4.57	PCUN	Right	3.47	PCUN	Right	4.31
CAL	Left	3.14	CAU	Left	4.37	OLF	Left	3.12	PCUN	Left	4.18
LING	Right	2.91	PCUN	Right	4.35	DCG	Right	2.88	PUT	Left	3.98
DCG	Right	2.70	HIP	Left	4.15	OLF	Right	2.35	HIP	Left	3.96
LING	Left	2.62	PUT	Right	4.08	INS	Left	2.32	PUT	Right	3.75
DCG	Left	2.38	SOG	Right	3.95	CAL	Left	2.16	CAL	Right	3.73
OLF	Left	2.21	MOG	Right	3.86	DCG	Left	2.11	SOG	Right	3.72
INS	Right	2.19	MOG	Left	3.84	IFGorb	Right	2.04	INS	Right	3.62
ACG	Left	2.19	CAL	Right	3.82	STG	Right	1.93	CAL	Left	3.55
CAL	Right	2.09	INS	Right	3.79	LING	Left	1.90	ACG	Left	3.51
OLF	Right	1.98	CAL	Left	3.76	INS	Right	1.84	MOG	Left	3.32
INS	Left	1.89	PreCG	Left	3.61				INS	Left	3.29
			PreCG	Right	3.54				PosCG	Right	3.29
			STG	Right	3.49				DCG	Left	3.17
			INS	Left	3.48						
			CAU	Right	3.45						
			DCG	Left	3.44						

b (*i*): The normalized nodal betweenness; *S* (*i*): The nodal strength. The regions in bold font were the hubs that identified by both *b* (*i*) and *S* (*i*). PreCG: Precentral gyrus; PosCG: Postcentral gyrus; IFGorb: Inferior frontal gyrus, orbital; OLF: Olfactory cortex; STG: Superior temporal gyrus; PCUN: Precuneus; CAL: Calcarine fissure and surrounding cortex; LING: Lingual gyrus; SOG: Superior occipital gyrus; MOG: Middle occipital gyrus; ACG: Anterior cingulate and paracingulate gyri; DCG: Median cingulate and paracingulate gyri; INS: Insula; PUT: Lenticular nucleus, putamen; CAU: Caudate nucleus; HIP: Hippocampus; HC: Healthy controls; MDD: Major depressive disorder.

threshold for multiple comparisons between MDD patients and HCs [Table 6].

Discussion

This study uses graph analyses and DTI data to compare the topological characteristics of the brain structural networks in HCs and MDD patients. We constructed a set of undirected weighted graphs for each subject and compared the topological properties of brain functional networks between the two groups. The results reveal that the brain structural networks in both groups followed an efficient small-world organization, which is consistent with several previous studies.[30,31,33,34] Nevertheless, we found disturbed topological properties of the brain structural network in MDD patients compared with those of healthy subjects.

The human brain has been described as a large and complex network of regions interconnected structurally by WM tracts, which has an economical, small-world architecture.[26,27] And it is characterized by the coexistence of structurally segregated and integrative connectivity patterns and has the ability of efficiently parallel information transfer at a relatively low cost.[30,31] The topology of this network assure that the brain generates and integrates information with high efficiency between brain regions.[35,36] In this study, both the brain structural networks of HCs and MDD patients have a higher clustering coefficient and a shorter characteristic path length when compared with the matched random networks. Many previous morphological, functional imaging and DTI studies have identified small-world topology of the brain networks in MDD.[20,21,37] Recent studies also show that the brain network of MDD has preserved small-world topological properties characterized by a high level of segregation and global efficiency.[38] And our results were consistent with several previous brain functional and structural network studies in MDD patients.[20,39]

Specifically, we found that, in contrast to healthy HCs, the brain structural network of MDD patients were characterized

Table 6: Abnormal nodal metrics in MDD patients as compared with healthy controls

Regions	*P*					
	$E_{glob}(i)$	$E_{loc}(i)$	*C* (*i*)	*L* (*i*)	*S* (*i*)	*b* (*i*)
Right rolandic operculum	0.00013*	0.023	0.27	0.19	0.016	0.52
Right supramarginal gyrus	0.00036*	0.051	0.30	0.044	0.081	0.60
Right angular gyrus	0.000064*	0.12	0.44	0.36	0.023	0.62
Right heschl gyrus	0.00018*	0.14	0.22	0.056	0.21	0.25
Left middle temporal gyrus (temporal pole)	0.00026*	0.070	0.38	0.40	0.0014	0.66

$E_{glob}(i)$: The nodal global efficiency; *S* (*i*): The nodal strength; *C* (*i*): The nodal clustering coefficient; *L* (*i*): The nodal characteristic path length; E_{loc} (*i*): The nodal local efficiency; *b* (*i*): The normalized nodal betweenness. Regions were considered abnormal in the MDD patients if their $E_{glob}(i)$ exhibited significant between-group differences ($P<0.05$, corrected, *That the regions survived critical FDR threshold for multiple comparisons). And the *P* values of other nodal measures of these nodes were also presented (the bold font *P* values mean that they exhibited significant between-group differences, $P<0.05$, uncorrected). MDD: Major depressive disorder.

by less specialized or segregated network organization, indexed by significantly lower average clustering coefficient and lower average local efficiency, which mean a trend to a less dense interconnection with neighbor regions.[40] This finding suggests that MDD patients is associated with reduced capacity for the regions to form cliques with other brain regions, which is likely to be associated with the generation of some symptoms of MDD patients. The path length and global efficiency of a node implies how close it is connected globally and how efficiency it transfer information globally to other nodes of the network, with shorter path lengths or higher global efficiency reflecting higher levels of information transfering efficiency.[31] So, our findings suggest that the brain structural network in MDD patients had decreased average global efficiency and decreased average strength of connectivity, implying a significant decrease of network connectivity of some brain areas and a disturbance of the normal global integration of whole brain networks.[39,41] This finding supports the hypothesis that MDD is a disorder of dysfunctional integration among large, distant brain regions.[14] And this finding may also suggest that MDD impacts the capacity of brain regions to efficiently integrate information across the brain network, which leads to a lower global efficiency of the network integration or a lower efficiency of the parallel information transfer in the brain structural network of MDD patients and then destructed the cognitive fitness and intelligence of the brain.[15,28,42] All these findings tend to suggest that MDD affects the global organization of the brain network and lead to a lesser locally and globally interconnected organization or a lesser strong connectivity of the overall level network.[31,43] Altered average clustering coefficient and local efficiency of the brain networks in MDD has also been reported. Previous DTI studies reported lower average clustering coefficient and lower average local efficiency in MDD.[44] However, some functional imaging studies reported that the average clustering coefficient of the brain networks in MDD was unchanged.[45] The results were consistent with some previous study that reported less strongly globally connected and less organized functional brain networks in MDD patients.[39] The findings about the average clustering coefficient and local efficiency of the brain networks in MDD were inconclusive. All of these findings need to be confirmed with larger samples.

Moreover, many local brain regions were profoundly affected, which were found in regions that have been implicated in dysfunction of emotion regulation and cognition in MDD patients. Specifically, MDD patients displayed a significantly decreased global efficiency of the right rolandic operculum, the right supramarginal gyrus, the right angular gyrus, the right Heschl's gyrus and the left middle temporal gyrus (temporal pole). As the global efficiency of a node expresses how closely it is connected globally to other nodes in the network and a higher global efficiency means a higher levels of efficient access to information,[31] our findings suggest a reduced global efficiency of frontal, parietal and temporal brain regions in MDD patients. And as the higher global efficiency of the network integration or the efficiency of the parallel information transfer in the network has been linked to cognitive fitness of the brain, this finding may also suggest that MDD impacts the capacity of frontal, temporal and parietal brain regions to efficiently integrate information across the brain network.[41] Together, these regional abnormalities might suggest an altered segregated network organization of different brain systems and lead to reduced global integration of information between widespread brain regions, which results in a disruptive integrated network organization of the brain structural networks in MDD patients. This further supports that these brain regions are also key regions of the brain structural network though they are not identified as hubs by the metrics normalized betweenness centrality $b(i)$ and strength of connectivity $S(i)$. And future studies examining the other regional topological properties of brain regions in MDD patients and their specific impact on structural and functional brain global network metrics are needed. Previous studies in MDD have reported decreased global efficiency in the whole-brain network, especially, in the frontal, parietal and temporal brain regions.[37,38,44] However, we did not find the very important brain, amygdala, which should be one of the major findings in previous functional imaging studies. We speculate that the sample size of this study is relatively small, while a larger sample size is needed to find more important brain statistically significantly.

The normalized betweenness centrality $b(i)$ and the strength of connectivity $S(i)$ are important metrics that have been adopted to assess the relative importance of a node and can identify the pivotal nodes in a network.[30,42] The hub regions are identified in central brain regions, which has been proven to play a central role receiving convergent inputs from multiple cortical regions and are involved in emotional processing and the maintenance of a conscious state of mind.[16,46] Relative to HCs, less hub regions were identified in MDD patients, showing loss of central cortex hubs and emergence of noncentral cortex hubs. And our findings also suggest a less strongly integrated structural brain network in MDD patients, with a reduced number and central role of key hubs. These brain regions have been reported to show morphological and functional changes in MDD patients.[43,47-50] This further supports that these brain regions have a strong impact on global information integration of the brain structural network in MDD patients and that they are key regions of the brain structural network. And the distribution of the key hubs in brain structural network of MDD is consistent with our previous result.[37]

In conclusion, our results of the graph theory analysis of the FA-weighted brain structural network in MDD patients support the concept that the brain structural network is a large and complex network with an optimal economical small-world topological property. Although MDD patients showed an overall intact small-world topology, significantly altered global topological organization and regional characteristic of the nodes in the frontal, parietal and temporal

areas of the brain structural network were found. Thus, the global network and regional node-level aberrations identified in the present study provide insights into our understanding of altered topological organization in functional brain networks of MDD patients in previous studies and may have important neurobiological implications for the pathophysiology of MDD from the view of the brain network.

Financial support and sponsorship

The work was supported by the grants from: The National High-tech Research and Development Program of China (No. 2015AA020509); the National Natural Science Foundation of China (No. 81571639, No. 81371522, No. 61372032); the Clinical Medicine Technology Foundation of Jiangsu Province (No. BL2014009); the Natural Science Foundation of Jiangsu Province (No. BK20131074); State Key Clinical Specialty (Psychiatry, 2011-873); and Provincial Medical Key Discipline (Psychiatry, 2011-12).

Conflicts of interest

There are no conflicts of interest.

References

1. Gotlib IH, Joormann J. Cognition and depression: Current status and future directions. Annu Rev Clin Psychol 2010;6:285-312. doi: 10.1146/annurev.clinpsy.121208.131305.
2. Culpepper L. Understanding the burden of depression. J Clin Psychiatry 2011;72:e19. doi: 10.4088/JCP.10126tx1c.
3. Hardeveld F, Spijker J, De Graaf R, Nolen WA, Beekman AT. Prevalence and predictors of recurrence of major depressive disorder in the adult population. Acta Psychiatr Scand 2010;122:184-91. doi: 10.1111/j.1600-0447.2009.01519.x.
4. Bora E, Fornito A, Pantelis C, Yücel M. Gray matter abnormalities in major depressive disorder: A meta-analysis of voxel based morphometry studies. J Affect Disord 2012;138:9-18. doi: 10.1016/j.jad.2011.03.049.
5. Sacher J, Neumann J, Fünfstück T, Soliman A, Villringer A, Schroeter ML. Mapping the depressed brain: A meta-analysis of structural and functional alterations in major depressive disorder. J Affect Disord 2012;140:142-8. doi: 10.1016/j.jad.2011.08.001.
6. Amico F, Meisenzahl E, Koutsouleris N, Reiser M, Möller HJ, Frodl T. Structural MRI correlates for vulnerability and resilience to major depressive disorder. J Psychiatry Neurosci 2011;36:15-22. doi: 10.1503/jpn.090186.
7. Cheng YQ, Xu J, Chai P, Li HJ, Luo CR, Yang T, *et al.* Brain volume alteration and the correlations with the clinical characteristics in drug-naïve first-episode MDD patients: A voxel-based morphometry study. Neurosci Lett 2010;480:30-4. doi: 10.1016/j.neulet.2010.05.075.
8. Korgaonkar MS, Grieve SM, Koslow SH, Gabrieli JD, Gordon E, Williams LM. Loss of white matter integrity in major depressive disorder: Evidence using tract-based spatial statistical analysis of diffusion tensor imaging. Hum Brain Mapp 2011;32:2161-71. doi: 10.1002/hbm.21178.
9. Yao Z, Wang L, Lu Q, Liu H, Teng G. Regional homogeneity in depression and its relationship with separate depressive symptom clusters: A resting-state fMRI study. J Affect Disord 2009;115:430-8. doi: 10.1016/j.jad.2008.10.013.
10. Norbury R, Selvaraj S, Taylor MJ, Harmer C, Cowen PJ. Increased neural response to fear in patients recovered from depression: A 3T functional magnetic resonance imaging study. Psychol Med 2010;40:425-32. doi: 10.1017/S0033291709990596.
11. Gilbert AM, Prasad K, Goradia D, Nutche J, Keshavan M, Frank E. Grey matter volume reductions in the emotion network of patients with depression and coronary artery disease. Psychiatry Res 2010;181:9-14. doi: 10.1016/j.pscychresns.2009.07.006.
12. Wen MC, Steffens DC, Chen MK, Zainal NH. Diffusion tensor imaging studies in late-life depression: Systematic review and meta-analysis. Int J Geriatr Psychiatry 2014;29:1173-84. doi: 10.1002/gps.4129.
13. Colloby SJ, Firbank MJ, Thomas AJ, Vasudev A, Parry SW, O'Brien JT. White matter changes in late-life depression: A diffusion tensor imaging study. J Affect Disord 2011;135:216-20. doi: 10.1016/j.jad.2011.07.025.
14. Leistedt SJ, Linkowski P. Brain, networks, depression, and more. Eur Neuropsychopharmacol 2013;23:55-62. doi: 10.1016/j.euroneuro.2012.10.011.
15. Bassett DS, Bullmore ET. Human brain networks in health and disease. Curr Opin Neurol 2009;22:340-7. doi: 10.1097/WCO.0b013e32832d93dd.
16. Bullmore E, Sporns O. The economy of brain network organization. Nat Rev Neurosci 2012;13:336-49. doi: 10.1038/nrn3214.
17. Rubinov M, Sporns O. Complex network measures of brain connectivity: Uses and interpretations. Neuroimage 2010;52:1059-69. doi: 10.1016/j.neuroimage.2009.10.003.
18. Ajilore O, Lamar M, Leow A, Zhang A, Yang S, Kumar A. Graph theory analysis of cortical-subcortical networks in late-life depression. Am J Geriatr Psychiatry 2014;22:195-206. doi: 10.1016/j.jagp.2013.03.005.
19. Jin C, Gao C, Chen C, Ma S, Netra R, Wang Y, *et al.* A preliminary study of the dysregulation of the resting networks in first-episode medication-naive adolescent depression. Neurosci Lett 2011;503:105-9. doi: 10.1016/j.neulet.2011.08.017.
20. Singh MK, Kesler SR, Hadi Hosseini SM, Kelley RG, Amatya D, Hamilton JP, *et al.* Anomalous gray matter structural networks in major depressive disorder. Biol Psychiatry 2013;74:777-85. doi: 10.1016/j.biopsych.2013.03.005.
21. Zhang J, Wang J, Wu Q, Kuang W, Huang X, He Y, *et al.* Disrupted brain connectivity networks in drug-naive, first-episode major depressive disorder. Biol Psychiatry 2011;70:334-42. doi: 10.1016/j.biopsych.2011.05.018.
22. Krieg SM, Buchmann NH, Gempt J, Shiban E, Meyer B, Ringel F. Diffusion tensor imaging fiber tracking using navigated brain stimulation – A feasibility study. Acta Neurochir (Wien) 2012;154:555-63. doi: 10.1007/s00701-011-1255-3.
23. Liu Y, Liang M, Zhou Y, He Y, Hao Y, Song M, *et al.* Disrupted small-world networks in schizophrenia. Brain 2008;131(Pt 4):945-61. doi: 10.1093/brain/awn018.
24. Tzourio-Mazoyer N, Landeau B, Papathanassiou D, Crivello F, Etard O, Delcroix N, *et al.* Automated anatomical labeling of activations in SPM using a macroscopic anatomical parcellation of the MNI MRI single-subject brain. Neuroimage 2002;15:273-89. doi: 10.1006/nimg.2001.0978.
25. He Y, Chen Z, Evans A. Structural insights into aberrant topological patterns of large-scale cortical networks in Alzheimer's disease. J Neurosci 2008;28:4756-66. doi: 10.1523/JNEUROSCI.0141-08.2008.
26. Watts DJ, Strogatz SH. Collective dynamics of 'small-world' networks. Nature 1998;393:440-2. doi: 10.1038/30918.
27. Latora V, Marchiori M. Efficient behavior of small-world networks. Phys Rev Lett 2001;87:198701. doi: 10.1038/30918.
28. van den Heuvel MP, Mandl RC, Stam CJ, Kahn RS, Hulshoff Pol HE. Aberrant frontal and temporal complex network structure in schizophrenia: A graph theoretical analysis. J Neurosci 2010;30:15915-26. doi: 10.1523/JNEUROSCI.2874-10.2010.
29. Maslov S, Sneppen K. Specificity and stability in topology of protein networks. Science 2002;296:910-3. doi: 10.1126/science.1065103.
30. Achard S, Salvador R, Whitcher B, Suckling J, Bullmore E. A resilient, low-frequency, small-world human brain functional network with highly connected association cortical hubs. J Neurosci 2006;26:63-72. doi: 10.1523/JNEUROSCI.3874-05.2006.
31. Achard S, Bullmore E. Efficiency and cost of economical brain functional networks. PLoS Comput Biol 2007;3:e17. doi: 10.1371/journal.pcbi.0030017.
32. Bullmore E, Sporns O. Complex brain networks: Graph theoretical analysis of structural and functional systems. Nat Rev Neurosci 2009;10:186-98. doi: 10.1038/nrn2575.
33. Bassett DS, Bullmore E. Small-world brain networks. Neuroscientist 2006;12:512-23. doi: 10.1177/1073858406293182.
34. Bassett DS, Meyer-Lindenberg A, Achard S, Duke T, Bullmore E. Adaptive reconfiguration of fractal small-world human brain functional networks. Proc Natl Acad Sci U S A 2006;103:19518-23. doi: 10.1073/pnas.0606005103.

35. He Y, Chen ZJ, Evans AC. Small-world anatomical networks in the human brain revealed by cortical thickness from MRI. Cereb Cortex 2007;17:2407-19. doi: 10.1093/cercor/bhl149.
36. Sporns O, Zwi JD. The small world of the cerebral cortex. Neuroinformatics 2004;2:145-62. doi: 10.1385/NI:2:2:145.
37. Qin J, Wei M, Liu H, Yan R, Luo G, Yao Z, *et al.* Abnormal brain anatomical topological organization of the cognitive-emotional and the frontoparietal circuitry in major depressive disorder. Magn Reson Med 2014;72:1397-407. doi: 10.1002/mrm.25036.
38. Korgaonkar MS, Fornito A, Williams LM, Grieve SM. Abnormal structural networks characterize major depressive disorder: A connectome analysis. Biol Psychiatry 2014;76:567-74. doi: 10.1016/j.biopsych.2014.02.018.
39. Park CH, Wang SM, Lee HK, Kweon YS, Lee CT, Kim KT, *et al.* Affective state-dependent changes in the brain functional network in major depressive disorder. Soc Cogn Affect Neurosci 2014;9:1404-12. doi: 10.1093/scan/nst126.
40. Kim DJ, Bolbecker AR, Howell J, Rass O, Sporns O, Hetrick WP, *et al.* Disturbed resting state EEG synchronization in bipolar disorder: A graph-theoretic analysis. Neuroimage Clin 2013;2:414-23. doi: 10.1016/j.nicl.2013.03.007.
41. Leow A, Ajilore O, Zhan L, Arienzo D, GadElkarim J, Zhang A, *et al.* Impaired inter-hemispheric integration in bipolar disorder revealed with brain network analyses. Biol Psychiatry 2013;73:183-93. doi: 10.1016/j.biopsych.2012.09.014.
42. Fischer FU, Wolf D, Scheurich A, Fellgiebel A. Association of structural global brain network properties with intelligence in normal aging. PLoS One 2014;9:e86258. doi: 10.1371/journal.pone.0086258.
43. Frodl T, Bokde AL, Scheuerecker J, Lisiecka D, Schoepf V, Hampel H, *et al.* Functional connectivity bias of the orbitofrontal cortex in drug-free patients with major depression. Biol Psychiatry 2010;67:161-7. doi: 10.1016/j.biopsych.2009.08.022.
44. Meng C, Brandl F, Tahmasian M, Shao J, Manoliu A, Scherr M, *et al.* Aberrant topology of striatum's connectivity is associated with the number of episodes in depression. Brain 2014;137(Pt 2):598-609. doi: 10.1093/brain/awt290.
45. Leistedt SJ, Coumans N, Dumont M, Lanquart JP, Stam CJ, Linkowski P. Altered sleep brain functional connectivity in acutely depressed patients. Hum Brain Mapp 2009;30:2207-19. doi: 10.1002/hbm.20662.
46. Hwang K, Hallquist MN, Luna B. The development of hub architecture in the human functional brain network. Cereb Cortex 2013;23:2380-93. doi: 10.1093/cercor/bhs227.
47. Connolly CG, Wu J, Ho TC, Hoeft F, Wolkowitz O, Eisendrath S, *et al.* Resting-state functional connectivity of subgenual anterior cingulate cortex in depressed adolescents. Biol Psychiatry 2013;74:898-907. doi: 10.1016/j.biopsych.2013.05.036.
48. Salvadore G, Nugent AC, Lemaitre H, Luckenbaugh DA, Tinsley R, Cannon DM, *et al.* Prefrontal cortical abnormalities in currently depressed versus currently remitted patients with major depressive disorder. Neuroimage 2011;54:2643-51. doi: 10.1016/j.neuroimage.2010.11.011.
49. Takahashi T, Yücel M, Lorenzetti V, Walterfang M, Kawasaki Y, Whittle S, *et al.* An MRI study of the superior temporal subregions in patients with current and past major depression. Prog Neuropsychopharmacol Biol Psychiatry 2010;34:98-103. doi: 10.1016/j.pnpbp.2009.10.005.
50. Taylor WD, Macfall JR, Boyd B, Payne ME, Sheline YI, Krishnan RR, *et al.* One-year change in anterior cingulate cortex white matter microstructure: Relationship with late-life depression outcomes. Am J Geriatr Psychiatry 2011;19:43-52. doi: 10.1097/JGP.0b013e3181e70cec.